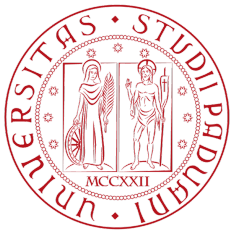


# UNIVERSITÀ DEGLI STUDI DI PADOVA

Dipartimento di Fisica e Astronomia “Galileo Galilei”

Corso di Laurea in Fisica


Tesi di Laurea

# Studio di fattibilità di un misuratore di emittanza 4D per la sorgente di ioni SPIDER

# Feasibility study of a 4D emittance measurement for the SPIDER ion source


Relatore

Dr. Gianluigi Serianni

Correlatore

Dr. Carlo Poggi

Laureando

Fabrizio Lovisetti



Anno Accademico 2022/2023

# Abstract

Magnetic confinement fusion may be one day a way to produce electrical power. However, a great quantity of energy is request for starting this process, and so an efficient way to heat the plasma in the reactor is needed. One method used by the ITER fusion experiment consists in neutral beam injectors (NBI), that are particle accelerators that produce intense beams of neutral hydrogen at high energy (1 MeV).

SPIDER is the prototype of the negative ion source of the ITER NBI, and it aims at producing up to 50 A of negative hydrogen at the energy of 100 keV divided in 1280 beamlet.

Optimizing the divergence of SPIDER beamlets will be useful in view of the operation of the full 1 MeV NBI. To this purpose, a thorough investigation of the beamlets optics is needed, and several diagnostics have been built for this purpose. A possible new diagnostic for reconstructing the entire transverse phase space of the beam is the 4D emittance scanner, an upgraded version of a previously existing sensor, the Allison scanner.

This thesis aims to prove the feasibility of this diagnostic, that is not obvious due to some technical issues. To reach this, the design of the scanner was studied with the help of some numerical simulations, that showed a promising prospective, and the results provided some optimal parameters for a possible detector for SPIDER.



# Sommario

La fusione a confinamento magnetico potrebbe essere un giorno un modo per produrre energia elettrica. Tuttavia, una grande quantità di energia è richiesta per innescare il processo, e quindi è necessario un modo per riscaldare il plasma in maniera efficiente. Un metodo usato nell'esperimento fusionistico ITER consiste negli iniettori di fasci di neutri (NBI), che sono acceleratori di particelle che producono intensi fasci di idrogeno neutro ad alta energia.

SPIDER è il prototipo della sorgente di ioni negativi degli NBI di ITER, e punta ad produrre più di 50 A di ioni negativi all'energia di 100 keV divisi in 1280 beamlet.

Ottimizare la divergenza dei beamlet di SPIDER sarà utile in vista del funzionamento dell'intero NBI all'energia di 1 MeV. Per raggiungere questo, un'adeguata analisi dei beamlet è richiesta, e diverse diagnostiche sono state costruite per soddisfare tale scopo. Una possibile nuova diagnostica per ricostruire l'intero spazio della fasi trasverso del fascio è lo scanner 4D di emittanza, che è una versione migliorata di un sensore precedentemente esistente, lo scanner di Allison.

Questa tesi vuole provare la fattibilità di questa diagnostica, che non è scontata visti diversi problemi tecnici. Al fine di raggiungere questo, è stato studiato il design dello scanner con l'aiuto di alcune simulazioni computerizzate, mostrando una prospettiva promettente, e i risultati hanno portato a individuare alcuni parametri ottimali per un possibile detector per SPIDER.

# Contents

# 1 Introduction

Magnetic confinement fusion is the most promising way to achieve nuclear fusion power. A plasma of deuterium and tritium is confined with the help of strong magnetic fields inside a toroidal chamber. The plasma is heated to temperature of about 150 million °C, and the nuclei gain enough kinetic energy to overcome the repulsion caused by the Coulomb force. The nuclei fuse, generating $^4$He and neutrons. Also thermal energy is released during the reaction, that can be converted in electric energy.

The most advanced experiment in magnetic confinement fusion will be ITER [1], the world's largest fusion machine, that has been designed to prove the feasibility of fusion energy production. ITER will use two external heating methods to supply energy to the plasma: with high frequency electromagnetic waves or with neutral beam injectors (NBI).

This second approach consists in accelerating negative hydrogen ions that are produced by a source. These ions travel in a vessel with low pressure gas, and so they are neutralized. The output is an intense beam of neutral particles at high energy that enters in the reaction chamber. The particles of the beam transfer their kinetic energy to the ones in the chamber, and this heats the plasma.

The MITICA experiment is the full-scale prototype of ITER NBI, and the SPIDER experiment is the prototype of the ion source of the particle accelerator. SPIDER aims at producing up to 50 A of negative hydrogen ions, divided in 1280 beamlets, and accelerate them up to 100 keV [2].

In SPIDER [3] eight different radio frequency drivers supply energy to a hydrogen plasma in an appropriated cylindrical cases in the rear part of the machine. Facing this region there is the plasma grid (PG), that is coated with caesium to increase negative ion production. The negative ions are then extracted from the plasma with the extraction grid (EG), that is at a potential of 10 kV higher compared to the PG. At the end, ions are accelerated towards the grounded grid (GG) to the energy of 100 keV. Magnetic filter is present in the system, to limit the extraction of electrons with the negative hydrogen ions.

The MITICA NBI is 25 m long, because the particle accelerator, located in the in the rear part of the machine, must be far away from the intense magnetic field of ITER. The smallest divergence of the beam has a huge effect at this distance, and so the single beamlet target divergence for MITICA is 7 mrad e-fold. Also, high current of the beam (the target is a current density of 300 A/m$^2$) is obtained if a sufficient number of negative ions is produced. To achieve this, the ion source must satisfy some requirements, and so it is important to optimize it whit the study on the SPIDER experiment.

Several diagnostics have been built to collect data about SPIDER, and one of this is an Allison 2D emittance scanner[4], that provides information about the position and velocity distribution of particles in only one direction transverse to the beam direction. However, the scanner can analyze the beam in only one transverse direction. The investigation of the other direction orthogonal to the beam is possible with another scanning, but no information about correlation between the two distributions would be obtained.

This information may be acquired by the 4D emittance scanner, an upgraded version of the Allison scanner that analyses simultaneously both transverse directions. However, several technical issues may compromise the feasibility of this diagnostic. For example, this detector measures currents that are much lower compared to one of the 2D emittance scanner and measuring at the same time the two transverse velocity is more complex. Also, the motion of such scanner would no longer be linear, but follow a path in two dimension.

For these reasons, a feasibility study and a first dimensioning of the 4D emittance scanner was required and is carried out in this thesis.

# 2 Basic theoretical concepts in particle accelerator physics

## 2.1 Phase space

The phase space [5] is defined as the space of the spatial coordinates and the corresponding momentum. For example, the space $(x, p_x, y, p_y, z, p_z)$ is the phase space associated with the three spatial coordinates $x$,$y$,$z$. However, in particle accelerator physics, in the case of continuous beams, where the longitudinal direction $z$ of the beam is not of interest, the beam is studied only in transverse directions.

Also, the ratios between the velocities in these directions and the velocity in the z direction, is small for a beam with small divergence. So, these ratios can be approximated (with Taylor expansion at first order) to the angles between the longitudinal directions (the $'$ symbol is used to indicate them):

$$x' = atan(\frac{v_x}{v_z}) \approx \frac{v_x}{v_z} \tag{1}$$

$$y' = atan(\frac{v_y}{v_z}) \approx \frac{v_y}{v_z} \tag{2}$$

This simplification is called *paraxial approximation*. In this situation, transverse angles are proportional to transverse momenta, and so the phase space $(x, x', y, y')$ is used instead of $(x, p_x, y, p_y)$. To visualize graphically the beam proprieties, often the distribution of particles is shown in the $(x, x')$ and the $(y, y')$ planes.

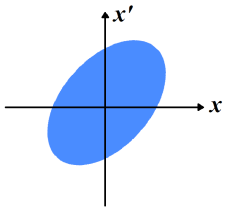


**Figure 1:** Example of phase space of a beam in two dimension: the width on the ellipse gives information about how much the beam is large in the x direction. The height of the ellipse determines how much the beam diverges

## 2.2 Particle distribution function

Studying a system with a large number of particles is impractical, because it would required to know positions and momenta of each atom or molecule. A macroscopic description of the system is necessary, that is provided by the particle distribution function $f(x_1, ...x_n, t)$, where $x_1, ..., x_n$ are the coordinates of the space phase that is the domain of this function. $f(x_1, ...x_n, t)dx_1...dx_n$ is the number of particles found at time t in the volume element $dx_1...dx_n$ around $(x_1...x_n)$ of the phase space. The function can be seen also as the probability density of finding a particle, satisfying the system constraints, in state $(x_1, ...x_n, )$ at time t, multiplied by the number of particles of the system. In the case of continuous beam, there is no dependency on time, and the transverse phase space is used, obtaining $f(x, x', y, y')$. Also the normalisation is redefined, so that the integral of the function over all the phase space is equal to one:

$$\int_\Omega f(x, x', y, y') = 1 \tag{3}$$

The beam distribution at a specific longitudinal position is described by the particle distribution function. If it is possible to factorize the function in two functions, each one referred to one direction:

$$f(x, x', y, y') = f_x(x, x')f_y(y, y') \tag{4}$$

The Gaussian distribution is a common approximation used to describe real beam in both $x$ and $x'$ coordinates (and also in $y$, $y'$)[5]:

$$f(x,x') = \frac{1}{2\pi\epsilon_x}\exp\left(-\frac{\gamma_x x^2 + 2\alpha_x x x' + \beta_x x'^2}{2\epsilon_x}\right) \tag{5}$$

$\alpha_x$, $\beta_x$ and $\gamma_x$ are known as the Twiss parameters. They can be different for the $x$ and the $y$ direction. The generic 4D Gaussian function, often used to modelling beams, is:

$$f(x,x',y,y') = \frac{1}{2\pi\epsilon}\exp\left(-\frac{\gamma_x x^2 + 2\alpha_x x x' + \beta_x x'^2}{2\epsilon_x}\right)\exp\left(-\frac{\gamma_y y^2 + 2\alpha_y y y' + \beta_y y'^2}{2\epsilon_y}\right) \tag{6}$$

## 2.3 Emittance

The emittance is defined as the phase space volume limited by a contour of constant particle density in the phase space. It will be indicated with $\epsilon$ if it is referred to the $(x,x',y,y')$ phase space, and $\epsilon_x$ or $\epsilon_y$ if it is refers to the $(x,x')$ or $(y,y')$ respectively. This volume obeys the Liouville theorem and is constant in conservative fields.

With practical accelerators, a more important beam quality measure is the volume inside the border surrounding the beam distribution because it is often non uniform. In two dimensions, for the Gaussian distribution contour is an ellipse, and it is used to calculate single direction emittance. The equation of this ellipse is:

$$\gamma_x x^2 + 2\alpha_x x x' + \beta_x x'^2 = \epsilon_x \tag{7}$$

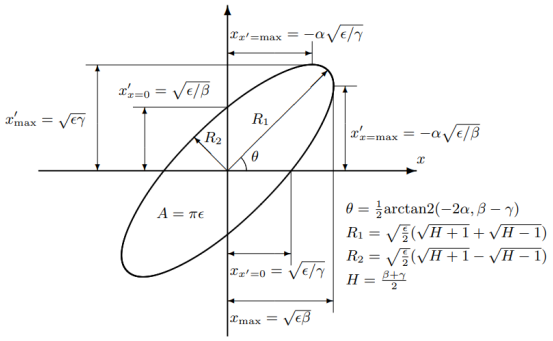


**Figure 2:** Ellipse contour of a Gaussian 2D distribution. Imagine from *Beam Extraction and Transport*, T. Kalvas [5]

with $\alpha_x$, $\beta_x$ and $\gamma_x$ defining the ellipse orientation and aspect ratio. Projecting on the two axis the 2D distribution, two one-dimension Gaussian distributions are obtained, one for the position and the other for the angle. The root mean square of the position distribution is $\sigma_x$, and $\delta_x$ for angle, that take the name of *divergence*. $\sigma_x$ and $\delta_x$ can be seen as the projections of the previous ellipse on the relative axis. They can be written as a functions of Twiss parameter:

$$\sigma_x = \sqrt{\epsilon_x\beta_x} \qquad\qquad \sigma_x = \sqrt{\epsilon_x\gamma_x} \tag{8}$$

Now that a contour is fixed, it is possible to calculate the emittance, that is the product of the two semi axes of the ellipse (**Figure 2**):

$$\epsilon_x = R1R2 = \frac{A_{ell}}{\pi} \tag{9}$$

To generalize to the four dimensions case, it is usefull to know that the total emittance is given by the product of the emittances in the two transverse directions:

$$\epsilon = \epsilon_x\epsilon_y \tag{10}$$

This is valid for every beam distribution that can be factorized in two distributions each one relative to a single dimension, like the four-dimensional Gaussian function used in **Equation 6**.

There will be a space standard deviation for the $x$ direction, $\sigma_x$, and another, in general different, $\sigma_y$. Analogously there will be two divergences $\delta_x$, $\delta_y$.

## 2.4 Beam distribution function changing along the longitudinal direction

If it assumed that particles drift not affected by any force and also that the beam is Gaussian, a simple relation can be found to provide the beam distribution function along the longitudinal direction. It is represented by the matrix $M$ that transforms the Twiss parameters, that define the Gaussian distribution from a known distribution:[6]:

$$\begin{pmatrix} \beta_L \\ \alpha_L \\ \gamma_L \end{pmatrix} = M \begin{pmatrix} \beta \\ \alpha \\ \gamma \end{pmatrix} = \begin{pmatrix} 1 & -2L & L^2 \\ 0 & 1 & L \\ 0 & 0 & L^2 \end{pmatrix} \begin{pmatrix} \beta \\ \alpha \\ \gamma \end{pmatrix} \tag{11}$$

## 2.5 The Allison 2D emittance scanner

The Allison scanner[4] is a diagnostic to reconstruct the distribution of a beam of particles in the phase space $(x, x')$. It measures the angular distribution of particles at different positions in one direction. It consists of three main parts:

- **Deflector**: It is a box with two aligned slits on opposite sides, that are larger than the beam diameter. Inside the box there is a pair of metal plates that can be polarized at opposite adjustable voltages. Particles enter from one slit and travel in the box. The electric field generated by the plates deflect the particles in a direction orthogonal to the beam direction (**Figure 3**). For a specific voltage value, only particles with a defined angle (see **Equation 14**) enter in the rear slit.
- **The Faraday cup:** the particles that exit from the rear slit are collected with the help of a metal electrode. However, particles strike the electrode with high energy, and so they generate secondary electrons, that induce a spurious current biasing the measured current. To fix this problem, a negatively polarized electrode is placed in front of the collector. It has a slit that allows the transit of the beam particles. The effect is the repulsion of the secondary electrons, that cannot escape from the collector and generate another current.
- **Handling system:** The voltages across the plate is varied, and the corresponding current is acquired, so an angle distribution of particles is obtained. This process is done for different positions in space with the help of the movement system, that moves the detector in the direction orthogonal to the beam direction (**Figure 4**).

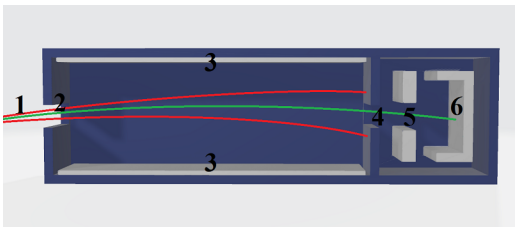


**Figure 3:** Part of the Allison scanner: 1-incident beam particle 2-front slit 3-plates 4-rear slit 5-repeller 6-collector. The green line is the trajectory of an accepted particle. The red lines represent particles that are not collected

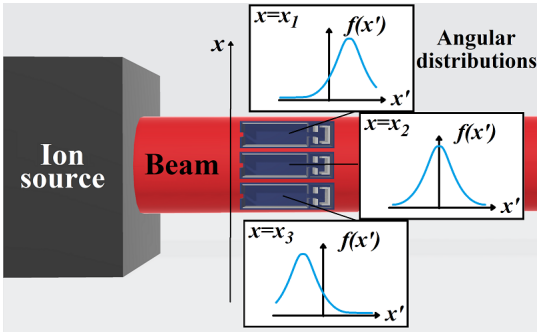


**Figure 4:** Working principle of the scanner: different $x'_0$ profiles are acquired at different positions

Let be $x_0$ the start position of a particle in the deflector in the transverse direction (assuming as zero the center of the slit) and $x_0'$ the start angle. The particle is affected by an electric field $E$, that can be assumed uniform in first approximation, in a region with a length $L$, that cause an acceleration $a_{elect}$. The slit width is $s$. Assuming the paraxial approximation, for which $v_x << v_z$, and neglecting the thickness of the deflector walls, the final position of the particle is $x_f$:

$$x_f = x_0 + x_0' L + \frac{1}{2} a_{elect} \Delta t^2 = x_0 + x_0' L + \frac{q \Delta V L^2}{4dU} \qquad x_f = x_0 + x_0' L + \eta \Delta V \tag{12}$$

Where $q$ is the charge of the particle, $\Delta V$ the drop across the plates, $d$ the distance between the plates, $U$ the kinetic energy of the particle. The multiplicative factor for $\Delta V$ is defined $\eta$. The condition for passing through the deflector is that $x_f$ is contained in the rear slit. Also $x_0$ must be in the same range of values because the particle starts from the front slit. This condition can be presented with some inequalities that define a parallelogram in the two dimensions phase space:

$$\frac{1}{L}(-\frac{s}{2} - x_0 - \eta \Delta V) < x_0' < \frac{1}{L}(\frac{s}{2} - x_0 - \eta \Delta V) \qquad -\frac{s}{2} < x_0 < \frac{s}{2} \tag{13}$$

The term $-\eta \Delta V$ can be interpreted as a vertical shift of the parallelogram (**Figure 5**). This can be interpreted as if different portions of the phase are accepted for different values of voltage.

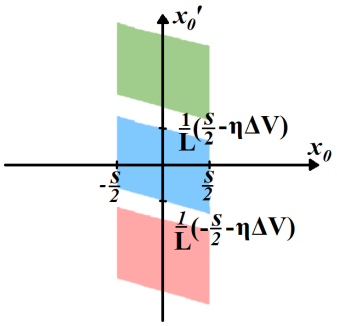


**Figure 5:** Accepted portion of the phase space as a function of the voltage difference. The green parallelogram is accepted for negative value of $\Delta V$. The red one, is selected for a positive value instead

If the total displacement in the $x$ direction during the motion of a particle is imposed to be zero, a simple relation can be found to define the angle at which particles are accepted:

$$x_0' = \frac{qVL}{4dU} \tag{14}$$

### 2.5.1 Acceptance

The concept of acceptance can be useful for a diagnostic that analyses the beam proprieties. The sensor accepts only particles that occupies in a specific portion of the phase space. The volume of this phase space region is the acceptance $A$.

The acceptance of the detector is given by the area of the phase space parallelogram:

$$A = \int_{d\Omega} dx_0 dx_0' = \int_{-\frac{s}{2}}^{\frac{s}{2}} dx_0 \int_{-\frac{h}{2}-x_0}^{\frac{h}{2}-x_0} dx_0' = \frac{s^2}{L} \tag{15}$$

## 2.6 Current measurement in SPIDER

An Allison emittance scanner was used in SPIDER to measure the parameter of 3 beamlets 0.6 m far away from the source. The distribution in position and angle were Gaussian like, but with larger tails. The divergence of a beamlet changes for different conditions from less than 20 to 30 mrad, and also the average density current varies between 50 and less than 200 $\mathrm{A/m^2}$[7] depending on the source parameters.

For the study of feasibility, the beamlets were modelled by approximating the beam distribution with a Gaussian function in four dimensions, with a value of divergence of $\delta = \delta_x = \delta_y$ = 15 mrad. $\sigma = \sigma_x = \sigma_y$ at the source was assumed as 3.5 mm, half the radius of the holes of the plasma grid of SPIDER. The average current density was assumed as 150 $\mathrm{A/m^2}$. The distribution at 0.6 m from the source (measurement condition) was found by assuming that the distributions in angle and position were not correlated at the source (upright condition), or rather $\alpha_x = \alpha_y = 0$. Then the assumption of linear drift of particles was applied (**Equation 11**) to find the Twiss parameters at 0.6 m from the source.

## 2.7 4D emittance scanner: working principle and application for SPIDER

The Allison scanner can provide information about the distribution of beam in one direction, and it is also possible to scan in the other transverse direction, but it is not possible to obtain information about the correlation between variables. This task may be performed by another sensor: the 4D emittance scanner. The concept is to upgrade the 2D scanner by replacing the slits with holes and adding another pair of plates, that are driven whit an independent voltage source, to deflect particles both transverse directions thus measuring both the $x'_0$ and $y'_0$ angle. Also, the detector has to be moved in the $x$ and $y$ direction to study in both spatial directions.

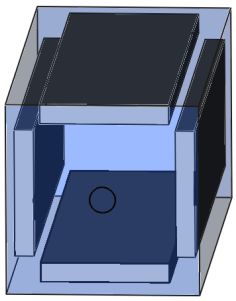

**Figure 6:** Sketch of the upgraded deflector to select particle in the $x$ and also in the $y$ directions

# 3 Desing of a 4D emittance scanner

## 3.1 Experimental requirements

A 4D emittance scanner can be used in SPIDER only if it satisfies some requirements. The goal is to have a diagnostic that can provide information about the beam distribution function. To achieve this, the scanner must have proper space and angular resolution. In the case of SPIDER a space resolution smaller than 0.5 mm and an angular resolution smaller than 1 mrad are needed, because the beamlets width is greater than 10 mm and their divergence reaches 20-30 mrad.

It is also necessary to have measurable current, the inferior limit on the detectable current can be assumed at 1 nA. This limit is not imposed by the amplifier gain, but by the noise induced by the radio frequency generator used to maintain the plasma in SPIDER.

If the scanner is used to measure near the centre of the beam and at small angles, it is possible to measure the highest values of current. However, when the scanner is used to measure the tails of the distributions, smaller currents are measured. Assuming that the beam is Gaussian distributed, information about the beam is obtained only if it is possible to measure until 2 standard deviations in the distribution of the four coordinates.

In the worst measurement condition, where the current is minimum, the detector is acquiring at $\pm 2\sigma$ in the space coordinates, and at $\pm 2\delta$ in the angular coordinates, assuming Gaussian beam distribution. If the current in this case is greater than 1 nA, it is possible to measure all the useful portion of the phase space of the beam.

In case the angular distributions present large tails (that are deviations from the Gaussian function) it is necessary that the deflector can handle particles with large angles, or rather in the range between -100 and 100 mrad.

Each beamlet carries a power of about 2 kW, so the scanner can be exposed for a short time to the beam to avoid excessive heating. For this reason, the scanner must be moved quickly. It is still object of study, but at the moment seems possible to reach the required velocity with a maximum payload of the handling system of 1 kg. Thus, the maximum length of the scanner must be 200 mm not to have a too heavy sensor.

## 3.2 Analytic calculation of diagnostic acceptance and resolutions

To study the main parameters of the detector a simple model of the deflector was defined. The preliminary study considered three parameters: (**Figure 7**)

- **s**: the side of the square hole in the front of the detector
- **h**: the side of the square hole in the rear of the detector
- **L**: the length of the detector

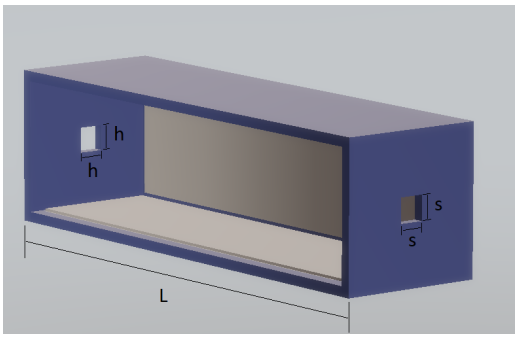


**Figure 7:** Simplify model of the deflector for preliminary study

To find the acceptance of the detector, it is possible to use an approach like the one used for the 2D scanner (see **Equation 13**). The motion of the particles can be studied separately in the

two transverse coordinates, and so we can find inequalities that define the particles that can come through the deflector for the $x$ direction:

$$\frac{1}{L}(-\frac{h}{2} - x_0 - kE_x) < x_0' < \frac{1}{L}(\frac{h}{2} - x_0 - kE_x) \qquad -\frac{s}{2} < x_0 < \frac{s}{2} \tag{16}$$

Note that $h$ appears in the first inequality instead of $s$ because the holes at the two sides can have different sizes. These relations are valid in the $y$ directions too:

$$\frac{1}{L}(-\frac{h}{2} - y_0 - kE_y) < y_0' < \frac{1}{L}(\frac{h}{2} - y_0 - kE_y) \qquad -\frac{s}{2} < y_0 < \frac{s}{2} \tag{17}$$

These inequalities describe a portion of a four dimensions phase space $d\Omega$. The differential symbol is used with $\Omega$ to remark that the portion of phase space is much smaller compared to the phase space occupied by the entire beam. The acceptance can now be calculated as an integral in four dimensions and can be interpreted as a four dimensional volume. Like before (**Equation 15**), the contribution from the term proportional to the electric field causes a shift of the phase space region, and so can be neglected for the volume calculation (complete calculation in Appendix **6.1**):

$$A = \int_{d\Omega} dx_0 dx_0' dy_0 dy_0' = \int_{-\frac{s}{2}}^{\frac{s}{2}} dx_0 \int_{\frac{1}{L}(-\frac{h}{2}-x_0)}^{\frac{1}{L}(\frac{h}{2}-x_0)} dx_0' \int_{-\frac{s}{2}}^{\frac{s}{2}} dy_0 \int_{\frac{1}{L}(-\frac{h}{2}-y_0)}^{\frac{1}{L}(\frac{h}{2}-y_0)} dy_0' = \frac{s^2h^2}{L^2} \tag{18}$$

Instead, resolutions of the detector can be estimated as the root mean square of corresponding variables, that can be calculated by using the definition of variance of a variable:

$$\sigma_\chi = \sqrt{var(\chi)} \qquad var(X) = \frac{\int_{d\Omega} \chi^2 \, dx_0 dx_0' dy_0 dy_0'}{\int_{d\Omega} dx_0 dx_0' dy_0 dy_0'} \tag{19}$$

Using $x_0$ and $x_0'$ instead of $\chi$ the spatial and angular resolution can be found (obviously calculation for $y_0$ and $y_0'$ are the same). For the explicit calculation check **Appendix 6.1**.

$$\sigma_{x_0,y_0} = \frac{s}{\sqrt{12}} \qquad \sigma_{x_0',y_0'} = \frac{\sqrt{s^2+h^2}}{L\sqrt{12}} \tag{20}$$

The spatial resolution depends only on the size of the front hole, and with the previous requirement an upper limit of 1.7 mm is fixed for $s$.

The current at specific coordinates, is given by the following relation:

$$I(x_0, x_0', y_0, y_0') = \int_{d\Omega} I_0 f(\tilde{x}_0, \tilde{x}_0', \tilde{y}_0, \tilde{y}_0') \, d\tilde{x}_0 d\tilde{x}_0' d\tilde{y}_0 d\tilde{y}_0' \tag{21}$$

where the constant $I_0$ is the total current of the beam. The tilde symbol is used to remark the difference between the integration variables, and the coordinates where the detector is measuring the current.

The scanner resolutions have to be smaller than the typical lengths and angles that characterized the beam distribution function. So the phase space portion $d\Omega$ that the detector accepts is very small compared to the total phase space of the beam. Hence, it is a good approximation to consider the beam distribution function as a constant value over the phase space $d\Omega$. This can simplify the calculation of the current:

$$I(x_0, x_0', y_0, y_0') \approx I_0 f(\tilde{x}_0, \tilde{x}_0', \tilde{y}_0, \tilde{y}_0') \int_{d\Omega} d\tilde{x}_0 d\tilde{x}_0' d\tilde{y}_0 d\tilde{y}_0' = I_0 f(\tilde{x}_0, \tilde{x}_0', \tilde{y}_0, \tilde{y}_0') \, A \tag{22}$$

With a fixed value of parameter L, the detector current is proportional to a factor $s^2h^2$ and the angular resolution to a factor $s^2 + h^2$:

$$A = \frac{s^2h^2}{L^2} \qquad \sigma_{x_0'} = \frac{\sqrt{s^2+h^2}}{L} = \text{const} \implies \sigma_{x_0'} = \frac{R}{L} \implies A = \frac{\sigma_{x_0'}^2 s^2h^2}{R^2} \propto s^2h^2 \tag{23}$$

It is possible to build a two dimensions space with $s$ and $h$ as coordinate. Fixing the angular error is visualized in this space like a quarter of circumference (considering only positive values for our parameters). Using polar coordinates it is possible to find the maximum of the current over this curve (using the unitary circumference):

$$s^2h^2 = \cos^2\theta \sin^2\theta = \frac{1}{4}\sin^2(2\theta) \qquad \theta \in [0, \frac{\pi}{2}] \tag{24}$$

It is easy to see that the current is maximized for $\frac{\pi}{4}$, or rather when the two hole sizes are equal, so from now on this case will be studied. The previous relation of acceptance and angle become:

$$A = \frac{h^4}{L} \qquad \sigma_{x_0,y_0} = \frac{h}{\sqrt{12}} \qquad \sigma_{x_0',y_0'} = \frac{h}{L\sqrt{6}} \tag{25}$$

The next step is to calculate the current in the worst measurement condition as a function of the two remaining parameters, $L$ and $h$, with the previous approximation to calculate current (**Equation 22**). Considering an average value of current density of 150 $\mathrm{A/m^2}$, the value $I_0$ of the total current is 23 mA (it is the area of the beamlet hole in the grid, multiplied for the density of current).

The beam distribution is approximated with the Gaussian function. The last element to define current is the acceptance, that is given as a function of $h$ and $L$ (**Equation 18**). The current in the worst measurement condition as a function of $h$ and $L$ in shown in **Figure 8**.

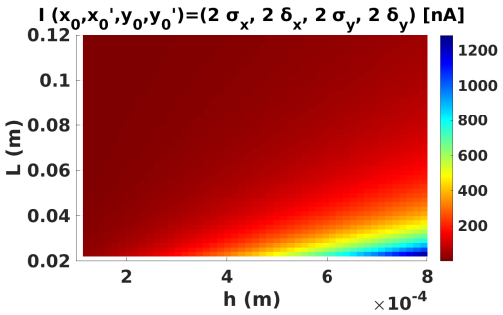


**Figure 8:** Current in the worst measurement condition in function of the length of the deflector and the size of the holes expressed with color gradient (nA)

Then all the values that produce a current under 1 nA are excluded, or rather the region in the left top corner. Also, all the parameter configurations that have an angular error above a specific threshold are removed. For the maximum limit of $h$ was found a large upper limit (spatial resolution), but the constraints from the angular resolution are more restrictive.

The parameter planes with constraints are shown in **Figure 9**, **Figure 10** and **Figure 11**, with different thresholds for the angular resolution:

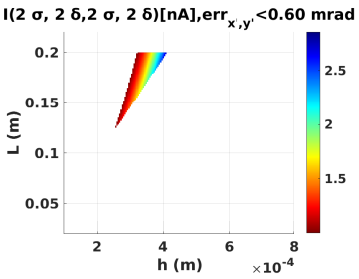


**Figure 9:** Plane of parameters restricted to the an angular error of 0.6 mrad

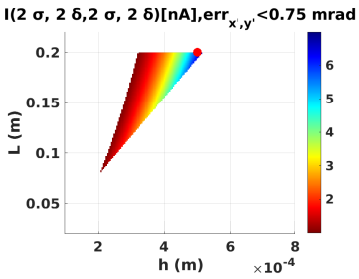


**Figure 10:** Plane of parameters restricted to the an angular error of 0.75 mrad. The red dot represents the best choose for the parameters

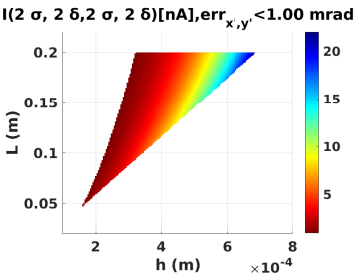


**Figure 11:** Plain of parameters restricted to the an angular error of 1 mrad

Plots suggest that choosing a lower angular error means having a lower current. So, the trade-off is to have an angular resolution of 0.75 mrad and a current in the worst condition of 8 nA, obtained with a length $L$ of 200 mm and a size of the hole of 0.5 mm (red dot in the graph in **Figure 10**).

With these values, the spatial resolution is 0.15 mm, that is smaller than the maximum limit of 0.5 mm.

## 3.3 Distance between plates and required voltages

Particles with large angles can collide on the plates of the deflector. This fact imposes a limit on the maximum analysable angle. So, an appropriate distance between the plates must be chosen.

The total displacement of an accepted particle in the $x$ direction can be written as:

$$\Delta x(t) \approx x'_0 L + \eta \Delta V = x'_0 v_z t + \frac{1}{2} a_{electr} t^2 \approx 0 \tag{26}$$

where $a_{electr}$ and $\eta$ were defined for **Equation 12**. The motion of particles in uniform electric field is parabolic. Let be $t_f$ the time needed for a particle to travel across the deflector. For accepted particles, $\Delta x$ must be zero (if the hole size is neglected) at $t_f$. So, the following relation can be written:

$$\Delta x(t_f) = x'_0 v_z t_f + \frac{1}{2} a_{electr} t^2 \approx 0 \implies \frac{1}{2} a_{electr} = -\frac{x'_0 v_z}{t_f} \tag{27}$$

The maximum displacement in the $x$ direction is reached at the time $\frac{t_f}{2}$:

$$\Delta x(\frac{t_f}{2}) = x'_0 v_z \frac{t_f}{2} - \frac{x'_0 v_z}{t_f} \frac{t_f^2}{4} = \frac{x'_0 v_z}{4 t_f} = \frac{x'_0 L}{4} \tag{28}$$

The particle with the maximum angle does not collide on the plate if the maximum displacement is equal to half the distance of the plates $d$. So, the maximum analysable angles are:

$$x'_{0,max} = y'_{0,max} = \frac{2d}{L} \tag{29}$$

To measure until 100 mrad, $d$ must be at least 10 mm. However, with this value, particles at large angles will explore regions of the electric field near the plates, where the field is far from being uniform. So, the relation between angle and voltage can be meaningfully different from a linear one. For reducing the impact of this effect, the chosen value for $d$ is of 20 mm. However, increasing this parameter increase also the maximum voltage required. Remembering the relation between angle and voltage (**Equation 14**), the maximum required voltage difference for $x'$=100 mrad is:

$$\Delta V_{max} = \frac{4 x'_{max} dU}{qL} = 2000V \tag{30}$$

that is a value that can be reasonably obtained with an appropriated power supply.

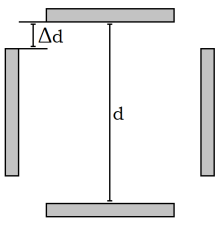


**Figure 12:** Section of the deflector with parameters to establish distance between plates

Another aspect that must be considered is the possibility of a discharge between plates. The shortest path for an electric discharge is between near plate, and the longest between opposite. To avoid this is important to estimate the breakdown voltage in the SPIDER condition with the Paschen theory, that gives the breakdown voltage as a function of the distance of electrode $d$ and pressure $p$:

$$V_b = \frac{Cpd}{ln \frac{Apd}{ln(1+\frac{1}{\gamma})}} \tag{31}$$

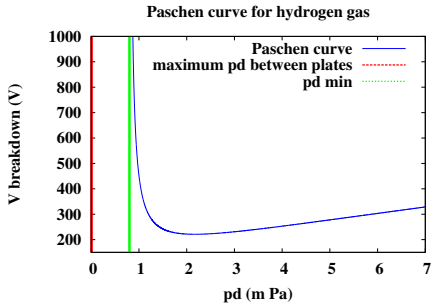


**Figure 13:** Paschen curve. The design product $pd$ is the left region of the graph, far from the curve minimum

The coefficient $A$, $C$ depend on the gas, $\gamma$ is the secondary electrons emission coefficient that depends also from the material of the electrodes.

The discharge can happen if the product $pd$ is larger than a certain value, $pd_{min}$:

$$pd_{min} = \frac{ln(1 + \frac{1}{\gamma})}{A} \tag{32}$$

With the typical hydrogen pressure in the SPIDER vessel of 50 mmPa, the product $pd$, also considering the maximum distance between plates, is much smaller compared to $pd_{min}$ (respectively $1 \cdot 10^{-3}$ Pa m and 0.8 Pa m).

The used values for A, C and $\gamma$ for hydrogen are A = 3.6 $Pa^{-1}$ $m^{-1}$, B = 102 V $Pa^{-1}$ $m^{-1}$ [9], $\gamma$ = 0.06 [10] (approximated value to find an upper limit). The pressure is so low that electrons cannot encounter enough gas particles to generate secondary electrons, that are needed for the start of the discharge.

However, the Paschen theory assumes a uniform electric field, a situation that is far from the one that can be expected in our deflector. Sharp edges can produce higher electric field that can start the discharge. Also, roughness of electrode material can heavily affect the $\gamma$ coefficient.

So, the previous comparison between $pd$ and $pd_{min}$ is intended as a rough calculation to check the possibility of discharge between plates.

For this reason, is necessary to keep a space of some millimetres between near plates, also to avoid unwanted short circuit. From the experimental campaign on SPIDER, a distance of three mm is known as safe for avoiding discharges between electrodes in a configuration similar to this one.

## 3.4 First study with numerical solution of Laplace equation: is it possible to obtain a voltage to angle map?

The previous analytic calculations were necessary to dimension the detector. However, the detector will have round holes instead of square one, because it is easier to drill holes in the metal plate. The chosen radius is $R$, that is equal to $\frac{h}{2}$ or rather 0.25mm. In this case the acceptance is slightly different, but the analytic calculations are more complex.

Another issue is the electric field: previously it was assumed to be the sum of the two ideal plain capacitor electric fields. This assumption can be well verified if the particles stay in the centre of the deflector, but particles with large angles can explore regions of the deflector that are dominated by fringe field effect of the plates. So, this effect can in principle lead to the impossibility to have a map that given the voltage differences at the plates returns the angles of the accepted particles. Finally, it can be useful to test how much the approximation of a uniform distribution function over the phase space $d\Omega$ affects the previous results.

To check the effect of this issues a simulation was made with the software MATLAB[11]. The main concept is to solve the Laplace equation in two dimensions (in the plain orthogonal to the motion of particle) for a specific voltage configuration. This gives the electric field for the $x$ and $y$ directions, and the field along $z$ is assumed null.

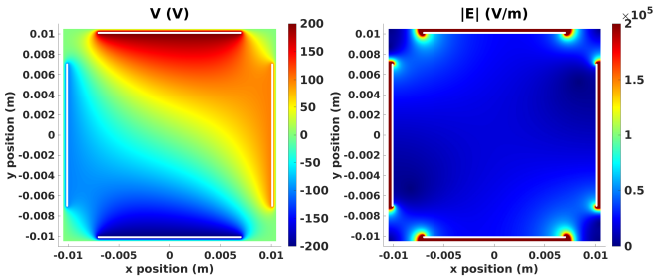


**Figure 14:** Electric potential and module of the electric field for $V_{TOP}$=200 V, $V_{RIGHT}$=100V obtained with a simulation in MATLAB

Then, the space position of the detector is assigned, that changes the angle distribution of particles (due to correlations of variables). With this distribution, many particles are generated, and their motion is simulated. The program repeats this process for many voltage configurations, and for each one counts how many particles are accepted and for which angles. The voltage configuration will be named with $V_{TOP}$ and $V_{RIGHT}$. They are respectively the voltage of the plate on the upper part of the deflector and on the right part of the detector if the observer is watching in the direction of motion of particles. Plates at opposite sides reach voltages that differ for a sign.

**Figure 15:** Idea of the simulation in MATLAB: many particles are generated, the trajectories are simulated and some particles are accepted

From the number of particles can be found the expected current $I_{simu}$ for a voltage configuration. This current is proportional to the fraction of the accepted particles in the simulation. The constant of proportionality $k$ is the total current of the beamlet multiply by the portion of the beam that is generated:

$$I_{simu} = k\frac{n_{simu,acc}}{n_{simu,tot}} \qquad k = I_0\frac{n_{beam,portion}}{n_{beam,tot}} = I_0\frac{\int_{d\Omega_{generate}} f(x_0, x_0', y_0, y_0')\, dx_0 dx_0' dy_0 dy_0'}{\int_{\mathbb{R}^4} f(x_0, x_0', y_0, y_0')\, dx_0 dx_0' dy_0 dy_0'} \tag{33}$$

Where $n_{simu,acc}$ is the number of particles accepted, $n_{simu,tot}$ the total number of generated particles, $I_0$ the total current of the beamlet, $d\Omega$ is the phase space volume in which particles are generated. The integration domain of the integral at the denominator is $\mathbb{R}^4$ because the Gaussian function is null at infinity. These integrals were calculated numerically.

### 3.4.1 Results at the centre of the beam

In **Figure 16**,**Figure 17** and **Figure 18** are shown results for the detector position of $(x_0, y_0) = (0, 0)$ mm, or rather at the center of the beam. Each coloured square represents the result of a simulation with a specific voltage configuration.

Some observations can be done. First, the angle for which the particles are collected in one direction is proportional to the voltage from a couples of plate and is nearly totally independent from the difference of potential between the other plates. This can be visualized for example for the $x_0'$ angle. Selecting a value of $V_{RIGHT}$ on the vertical axis, the angle $x_0'$ represented by the colour map is constant for different values of $V_{TOP}$ (maximum difference of 0.5 mrad). A similar relation is valid for $y_0'$. This linear relation is shown in **Figure 19**.

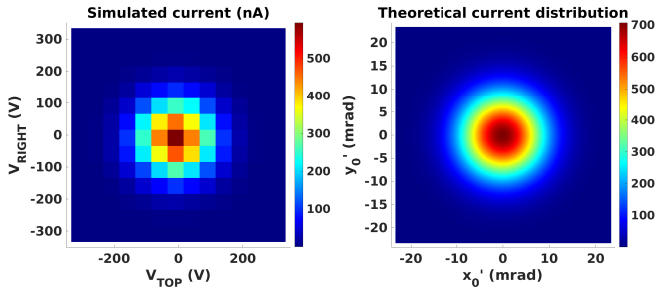


**Figure 16:** Current for each voltage configuration, simulated for $V_{TOP}$ and $V_{RIGHT}$ in the range [-300:300] V

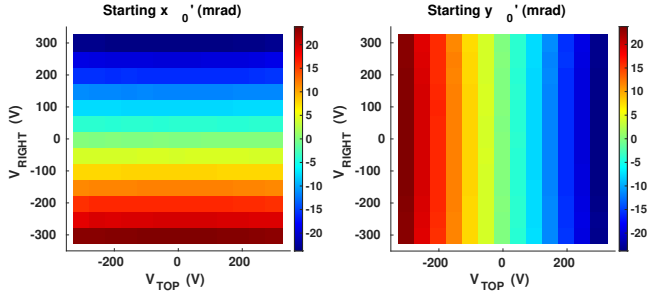


**Figure 17:** Voltage-angle map for $V_{TOP}$ and $V_{RIGHT}$ in the range [-300:300] V

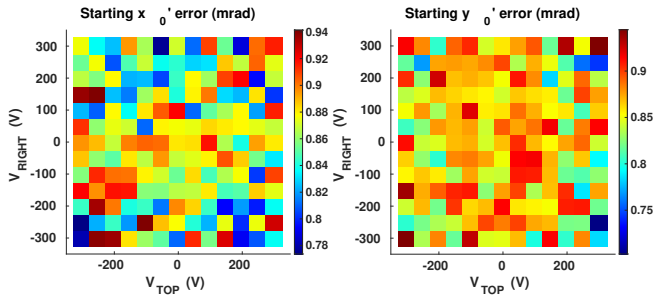


**Figure 18:** Angular error for $V_{TOP}$ and $V_{RIGHT}$ in the range [-300:300] V

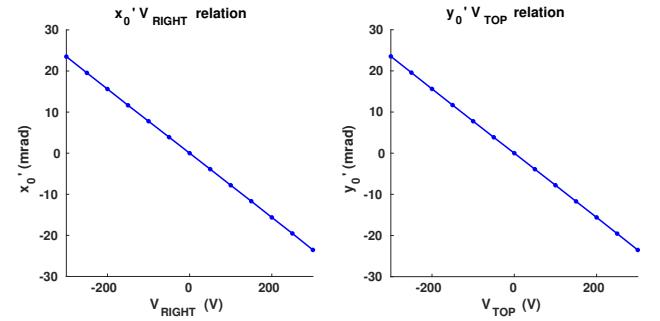


**Figure 19:** Relation between average single angles and their relative voltage. The difference in angle for different values of the other voltage is so small that cannot be visualized on the graph

So, it seems that there is a linear relation between angles and voltages. So, the current map presents values of current that are proportional to the distribution of particles as a function of angles, and it is in fact a two dimensions Gaussian distribution. Instead, the angular error maps show that the error is near to what was found in analytic calculation for square holes. There are some fluctuations of the error along $V_{RIGHT}$ and $V_{TOP}$, but they are caused by the finite number of particles in the simulation. The main information from this graph is that the error seems constant

over different voltages.

A parameter that is possible to deduce from the plot is the maximum current that the current detector must handle, and that is in the centre of the Gaussian distribution of current, or rather 550 nA.

### 3.4.2 Results in the worst measurement condition

Another simulation was done, this time at the space coordinates of $(x_0, y_0) = (2\sigma_x, 2\sigma_y)$, for investigating the current in the worst measurement condition. The range of $V_{TOP}$ and $V_{RIGHT}$ was changed to better investigate the significant region, and they are no more centered in zero (due to correlation of angle and position, at the side of the beam the mean angle is not null).

The voltage map (**Figure 21**) suggests in this situation a little correlation between angles in one direction and the electric field in the other direction. However, this contribution seems small, and is possible to find a linear relation between angles and voltages in first approximation. This is remarked by the graph in **Figure 22** where the maximum, the minimum and the average angles are accepted for each value of the associated voltage.

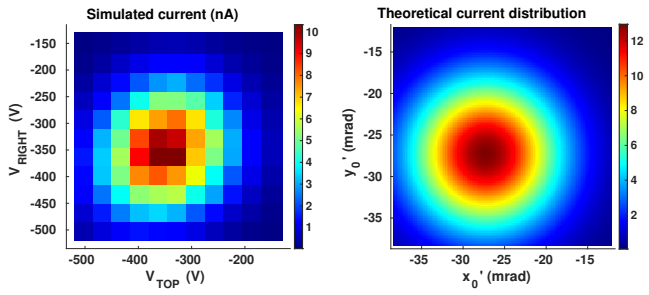


**Figure 20:** Current for each voltage configuration when the detector is in the position $(x, y) = (2\sigma, 2\sigma)$ for $V_{TOP}$,$V_{RIGHT}$ in the range [-500:-150] V

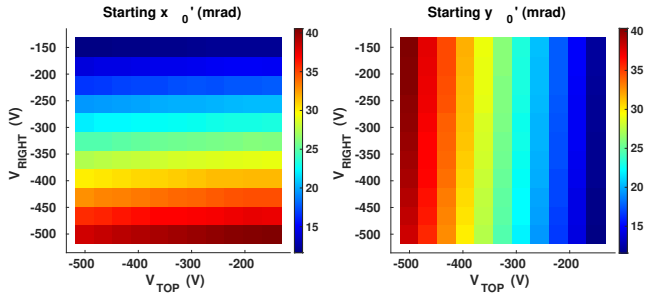


**Figure 21:** Voltage-angle map when the detector is in the position $(x, y) = (2\sigma, 2\sigma)$ for $V_{TOP}$,$V_{RIGHT}$ in the range [-500:-150] V

In (**Figure 23**) is shown a plot of the simulated current for different values of accepted angles. All the currents under 1 nA were removed. The red circle is the portion of the Gaussian angles distribution that is before 2 standard deviations from the centre. With the current limit of 1 nA it seems possible to investigate all this portion of the angular distribution. Also the angular errors is similar to the previous simulation (**Figure 24**).

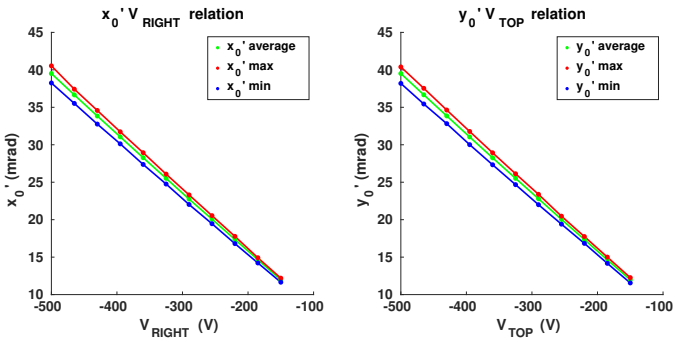


**Figure 22:** Angles in function of their relative voltage. Due to dependency also on the other voltages, the maximum, minimum and average angle is plotted. Obtained when the detector is in the position $(x, y) = (2\sigma, 2\sigma)$ for $V_{TOP}$,$V_{RIGHT}$ in the range [-500:-150] V. The dependency of angles from the other voltages is visible, because is more significant compared to **Figure 19**

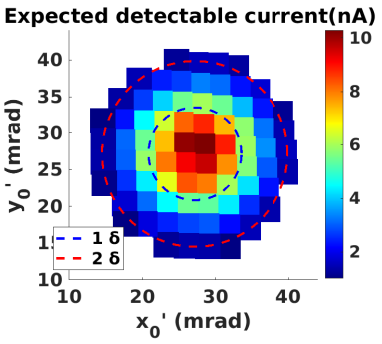


**Figure 23:** Current in the worst measurement condition. All the undetectable currents under 1 nA are removed. The values of divergence are shown in the graph

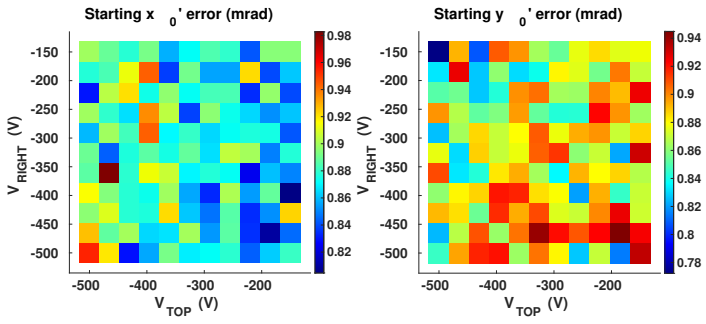


**Figure 24:** angular errors when the detector is in the position $(x, y) = (2\sigma, 2\sigma)$

### 3.4.3 Acceptance

The acceptance of the detector with square holes is equal to:

$$A = \frac{h^4}{L^2} = 1.56 \text{ mrad}^2\text{mm}^2 \tag{34}$$

It is also possible to calculate the acceptance with the MATLAB simulation for circular holes, generating particle with uniform angular distributions. The ratio between the number of particles accepted and the total one is equal to the ratio of the volume of the accepted phase space (acceptance) and the total phase space of the generated beam inside the deflector. This one is known, because it is the area of the front hole multiplied with angular amplitudes of the uniform beam:

$$A = \pi r^2 \Delta x' \Delta y' \frac{n_{part,accep}}{n_{part,tot}} \tag{35}$$

The acceptance is subjected to some fluctuation for different voltages due to the finite number of particles (**Figure 25**).

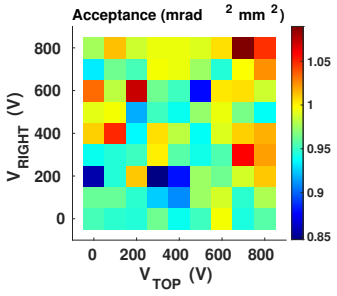


**Figure 25:** Numerically calculated acceptance for different voltages

The average value is 0.98 $\text{mrad}^2\text{mm}^2$, that is smaller than the one for square holes, which is coherent with the fact that the circle has an area smaller compared to the square, if the diameter is equal to the side size.

The acceptance, for squared holes, is proportional to the square of the area of holes. If it was true also for the circular holes, the ratio between the square case acceptance and the circular case acceptance would be the square of the ratio between areas of the two figures (about 1.62), that is close to the ratio found numerically (1.59). However, without an analytic formula of the acceptance for the round case, a formal conclusion cannot be achieved.

### 3.4.4 Gaussian profile reconstruction

The finite resolutions of the scanner cause small deformation of the measured distribution. In order to show that these deformations are negligible, in **Figure 26** on the left side is shown the reconstructed Gaussian distribution of the $y'_0$ angle with $x'_0 = 0$ mrad and with the detector at one specific space position $(x_0, y_0) = (0, 0)$ mm. In the right side is shown instead the graph of the spatial beam distribution in the $x$ direction, with $y_0 = 0$ mm and $x'_0 = y'_0 = 0$ mrad. The simulation were made with different values of divergences, in a view of possible measurement scenarios on SPIDER.

For each of the two situation, the Gaussian profiles are well visible and the distortions are really small.

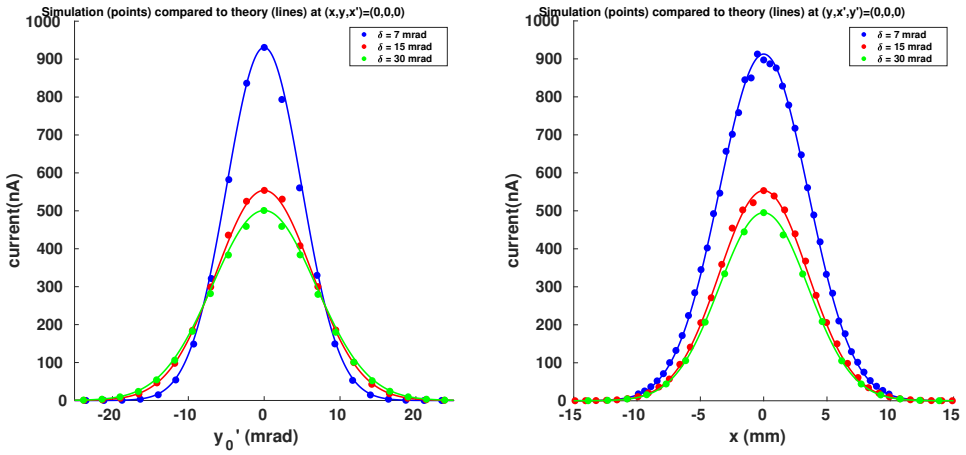


**Figure 26:** Simulation of the 1d profile reconstruction for $y_0'$ and for $x$ (dots). Lines represent the theoretical distribution

## 3.5 3D electric field and fringe field effects: simulation in COMSOL

In the previous simulation the electric field was assumed null in the direction of motion of particles, and this is not well verified at the ends of the deflector. So, for an investigation of a three-dimension electric field a new tool is needed.

For a more complete study, a model of the deflector was designed in COMSOL Muliphysics [12]. In fact, the electric field is close to the one found with the 2D simulation in the centre region of the deflector but is affected by fringe field effect in the terminal regions. The simulation in COMSOL aims to answering two questions: firstly, if this effect meaningfully changes the voltage-angle relation, and in second place, how large is this effect as function of the distance of plates from the front and rear walls of the deflector.

To achieve this, a beam of particles was simulated inside the deflector for different voltage configuration. As only the accepted angle dependency on voltages is needed, and not the collected current, the beam had a uniform distribution in angle. Also, the front and the rear walls of the deflector were imposed ground potential, to obtain a realistic electric field at the external region of the deflector.

In **Figure 27** the maps obtained with COMSOL are shown for an large range of values of voltage. Instead in **Figure 28** the difference between the two simulations are reported. The difference increases with voltages, but is always under 2 mrad, so the fringe field effect is not so relevant. Negative values of voltages are not reported because the voltage map is symmetric.

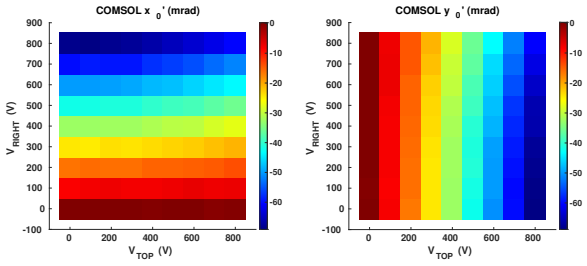


**Figure 27:** COMSOL angles-voltages maps

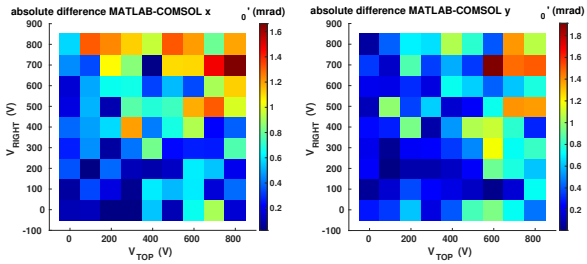


**Figure 28:** Differences of the voltages map in MATLAB and COMSOL

In **Figure 29** on the left side is shown the relation between the angles $x'_0$ (average, maximum and minimum) and some values of $V_{RIGHT}$ for the MATLAB simulation. On the right is presented the same relation for the COMSOL simulation.

Now, it is possible to study the influence of the fringe field effect as a function of the distance of the plates from the front and rear walls of the deflector. This parameter will be named $\Delta L$. The goal is to choose a parameter $\Delta L$ for which the deflection in not heavily affected, but also big enough to avoid discharges between plates and walls and undesired short circuits.

Increasing $\Delta L$ means reducing the length of the plates, and this causes a reduction of the size of the region with an electric field, resulting in a decrease of angle accepted for a fixed voltage. It is possible to write the equation of motion for particles (for example in the $x$ direction) inside the

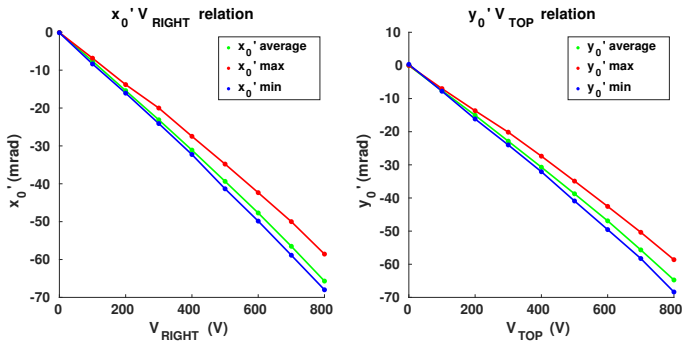


**Figure 29:** Comparison between the two angle-voltage relations from different simulations

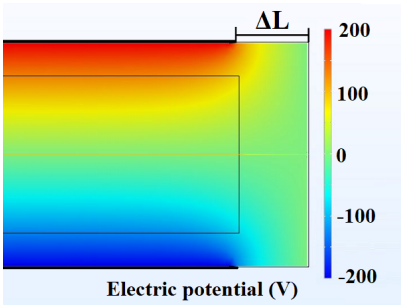


**Figure 30:** Section of the electric potential (V) provide by COMSOL for $V_{TOP} = 200V$ and $V_{RIGHT} = 100V$ and for $\Delta_L$=8 mm. It is possible note the fringe field in the final region.

deflector (**Equation 12**), considering that the electric field region is located only along the length of the plates:

$$x_f = x_0 + x_0' L + \frac{q\Delta V (L - 2\Delta L)^2}{4dU} \tag{36}$$

For passing particles $x_0$ is roughly equal to $x_f$, and so the accepted angle is:

$$x_0' = \frac{q\Delta V (L - 2\Delta L)^2}{4dUL} \propto \frac{(L - 2\Delta L)^2}{L} \tag{37}$$

The relative difference $D_r$ of accepted angles with $\Delta L$ different from zero and $\Delta L$ equal to zero is given by the following relation:

$$D_r = \frac{x_0' - x_{0,\Delta L=0}'}{x_{0,\Delta L=0}'} = \frac{(L - 2\Delta L)^2 - L^2}{L^2} = 4\Delta L \frac{\Delta L - L}{L^2} \approx -4\frac{\Delta L}{L} \tag{38}$$

$D_r$ is a useful parameter to investigate how much the deflection ability of the detector is affected. However, the previous calculation does not include fringe field effects, and so a simulation in COMSOL is required to calculate $D_r$.

Two cases were considered, one with $(V_{TOP}, V_{RIGHT}) = (200V, 0)$ (to analyse the cases of one polarized pair of plates, (**Figure 31**) and one with $(V_{TOP}, V_{RIGHT}) = (200V, 200V)$ (general case, **Figure 32**)

In both cases, the simulated value of $D_r$ seems smaller in module compared to the analytic one. This can be explained by the fact that at the end regions of the deflector there is a fringe field, that causes some orthogonal displacement that is not taken in account with the uniform field region approximation. Increasing the value of $\Delta L$ stretches the end region affected by the fringe field effect, increasing the effect on transverse displacement of particles. And so the decrease of deflection due to the reduction of plate length is partially compensated by this effect.

However, to have an acceptable angle reduction (1% at most), a value of 3mm was chosen for the parameter $\Delta L$.

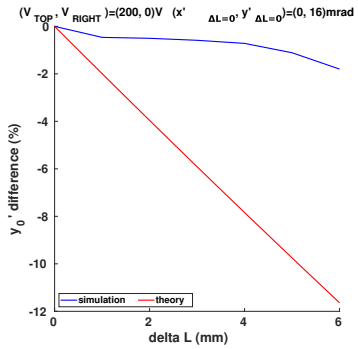


**Figure 31:** Percent difference of the accepted angle as a function of the parameter $\Delta L$ for $(V_{TOP}, V_{RIGHT)} = (200V, 0)$

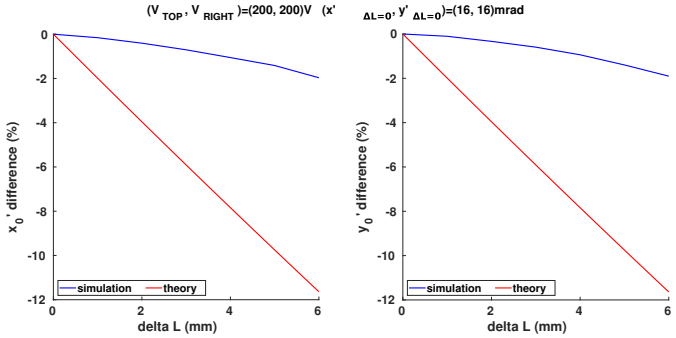


**Figure 32:** Percent difference of the accepted angle as a function of the parameter $\Delta L$ for $(V_{TOP}, V_{RIGHT)} = (200V, 200V)$

## 3.6 Divergence of the beam due to space charge

A beam of charged particles diverges due to its own space charge. This phenomenon can happen inside the scanner and can lead to a reduction of the measured current. In fact, the portion of beam inside the deflector that is accepted, can be schematized as a uniformly charged conoid, with a start radius equal to the one of the front hole.

The surface of the section of this conoid increases at the end of the deflector, due to the coulomb repulsion. The rear hole is smaller than this section, and so only a fraction of particles are accepted, leading to a reduction in current.

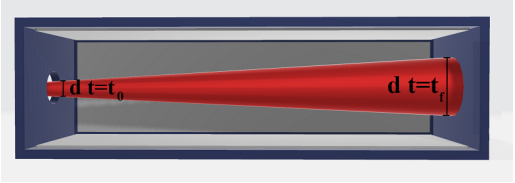


**Figure 33:** Conoid of particle that diverges due to space charge (not in scale)

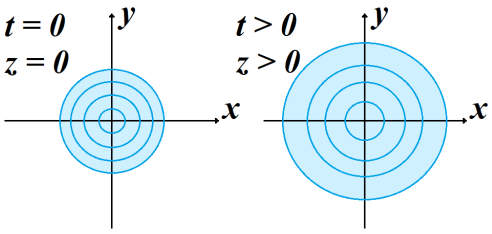


**Figure 34:** The idea to solve the problem: the section of the conoid is made by several infinitesimal circular crown that enlarge in time

To study this problem, the section of the cylinder can be assumed as made of many infinitesimal circular crowns and the charge is assumed distributed uniformly along the radii. It is also assumed that electric force is always radial, that is well verified for small radius increase of the section. The electric field that acts on the particles of the last circular crown can be calculated with the formula for a cylindrical distribution of charge for distance $r$ greater of the radius $R$ of the cylinder:

$$E = \frac{\lambda}{2\pi\epsilon_0 r} \tag{39}$$

where $\lambda$ is the linear charge density, and this expression is independent from the radial distribution of charge. So, the motion of the more external circular crown is uncorrelated from the motion of the inner ones (unless they become bigger than the external crown, but this is not possible because the acceleration on crowns increases with the radius). The radial acceleration of the particle of the last crown is:

$$a_r = \frac{F}{m} = \frac{qE}{m} = \frac{\lambda q}{2\pi\epsilon_0 m r} \tag{40}$$

Now the constants $c$ and $k$ are defined:

$$c = \frac{\lambda}{2\pi\epsilon_0 m} = \frac{j{r_0}^2 q}{2\epsilon_0 m v_z} \qquad k = \frac{j{r_0}^2 q}{2\epsilon_0 m {v_z}^3} \qquad c = k{v_z}^2 \tag{41}$$

where $j$ the density current, and $v_z$ the velocity of particles in the direction of the beam. This brings to a differential equation whose solution is $r(t)$, that is the external radius of the conoid as a function of time of motion of particle from the configuration in which the radius was the minimum, $r_0$. The equation is:

$$\frac{d^2 r(t)}{dt^2} = \frac{k}{r(t)} \qquad r(t=0) = r_0 \qquad \frac{dr(t)}{dt}(t=0) = 0 \tag{42}$$

The equation is more practical as a function of the longitudinal distance from the origin of the beam, obtaining the solution $r(z)$. This can be written with the constant $k$:

$$\frac{d^2 r(z)}{dz^2} = \frac{k}{r(z)} \qquad r(z=0) = r_0 \qquad \frac{dr(z)}{dz}(z=0) = 0 \tag{43}$$

This system does not admit analytic solution, but it is possible to write a Taylor expansion of the solution centered in zero:

$$r(z) = r_0 + \frac{k}{2r_0} z^2 - \frac{k^2}{24{r_0}^3} z^4 + o(z^5) \tag{44}$$

With an energy of particles of 50 keV, and a length and density current of 150 $\mathrm{A/m^2}$ and an initial radius of 0.25 mm, the final radius at 200m is 0.37 mm.

To study how the radial distribution is affected, it is necessary to remark that the motion of the inner circular crown is independent from the more external crown. So, for each crown, it is possible to write a different differential equation, that gives the final radius (that is indicated with the label $i$):

$$\frac{d^2 r_i(z)}{dz^2} = \frac{k_i}{r_i(z)} \qquad r_i(z=0) = r_0, i \qquad \frac{dr(z)}{dz}(z=0) = 0 \tag{45}$$

Is possible to define the constants $k' = \frac{k_i}{r_{0,i}}$ that is equal for all the circular crowns, so it is explicit that the final radius of a single crown is proportional to the initial value of the radius:

$$r(z)_i = r_0 \left(1 + \frac{k'}{2} z^2 - \frac{k'^2}{24} z^4 + o(z^5)\right) = r_0 g(z) \tag{46}$$

So, a initial radial distribution profile, is preserved from the divergence of the beam, and in this case, the final distribution of charges is also uniform. With this information, the portion of particles accepted at the rear hole is equal to the ratio between the radius of the hole and one of the final section, that causes a current reduction of the 55%

This problem was also studied with a simulation in the software COMSOL Multiphysics. The result whit the same condition of before is a final radius of 0.33 mm, and a corresponding current reduction of the 44%.

However, this factor has to be intended as the one in worst case scenario. In fact, particles are slightly divergent due to the presence of an angular distribution, so they distance each other and the global repulsion decreases.

Another important factor is space charge compensation[5][8]The potential well of the beam formed by the positive charged particles acts as a trap for electrons produced in the background gas ionization due to the beam. The trapped electrons compensate the charge density of the beam, decreasing the depth of the potential well and therefore also decreasing the magnitude of the divergence to the space charge.

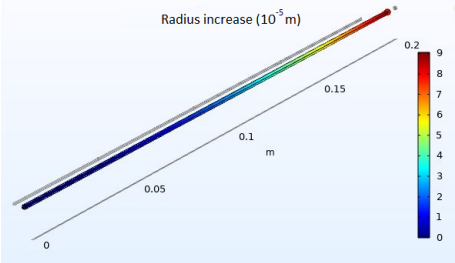


**Figure 35:** Simulation in COMSOL of the divergence of the beam inside the deflector due to space charge

## 3.7 Sampling rates

Another aspect to consider for the application for measure on SPIDER is the sampling rate of the current. In fact, measuring at the same time both angular distributions with enough precision, while the scanner is moved in both directions, can be challenging. The main problem is that the time for the measure is limited by the temperature increase of the detector due to the energy given by the beamlets.

Now the best estimation of the maximum time of measure, is of about 100 s. In this time, the detector must move through a path length 0.9 m with a serpentine shape like.

To use at best the the spatial resolution of the detector, a measure of the angular distribution must be done in a length of 0.15 mm (the previous assigned error). This implies a rate of the angular measure of 60 Hz.

For each one of this, the voltage across one pair of plates goes from the minimum to the maximum value with a ramp shape signal. At the same time, the voltage on the other pair follows a signal with a triangular wave, with a frequency higher than the one of the ramp.

For each half period of the triangular wave, a minimum of 20 measures in current must be acquired (for having 20 values of angular distribution for one angle). Also, in the period of the ramp, 20 groups of measure must acquire for having 20 values for the other angles.

In total, 400 current measures are done with a frequency of 60 Hz, or rather the global sampling rate is of 24 kHz, that is a frequency range allowed for many amplifiers and analog to digital converters.

However, the maximum time for the measure is still object of study, because it depends on the final geometry and material of the scanner, that will be decided in the future considering also the building practical limits.

Also, the handling system is currently under development, because it is challenging to move an object in vacuum with great precision, repeatability and in both transverse directions.

### 3.7.1 Faraday cup: design and current measurement requirements

For collecting the accepted particle, a Faraday cup is required. As said before in **Section 2.5**, this is made by a charge collector and a repeller, to avoid measuring a fake current due to secondary electrons. The repeller is a square of metal plate, with a hole in the centre, with a radius that is larger than the ones in the deflector wall. The collector, instead, is a parallelepiped, with a conic hole at the centre of one face. The holes of the repeller and of the collector have their centre aligned on the same axis, and the two components are some millimetres away from each other (**Figure 36**).

The reason for the conic hole in the collector is to avoid the escaping of secondary electron and of sputtered ions from the metal material of the collector. In fact, the conic geometry reflects the majority of this unwanted particles inside the cone, avoiding them from escaping.

In view of measurement in SPIDER, the polarization of the repeller must be up to -500 V, because secondary electrons can have high energy, due to high energy of incident ions. A computational simulation showed how 200 V are enough[13] to repel all the secondary electrons, but the polarization can be increased for caution.

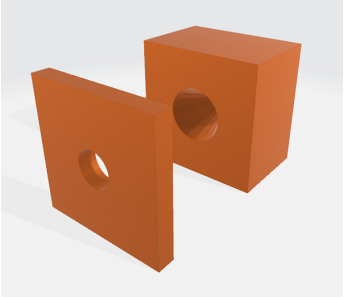

**Figure 36:** Faraday cup for the 4D emitter scanner. On the left: the repeller. On the right: the collector

## 3.8 Detector parameters for SPIDER

### 3.8.1 Deflector: plates, voltages, sampling rates

Summarising, the optimal geometrical parameter for the scanner, found previously, are:

- **Length L:** 200 mm
- **Diameter of holes R:** 0.5 mm
- **Distance of opposite plate d:** 20 mm
- **Distance of plates from lateral walls $\Delta d$:** 3 mm
- **Distance of plates from front and rear walls $\Delta L$:** 3 mm
- **Plates surface:** 196x16 mm
- **Maximum required voltage drop required:** 2000 V
- **Maximum frequency for voltage driver:** 180 Hz

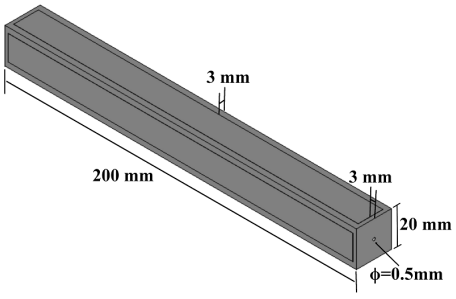


**Figure 37:** Sketch of the deflector with values of the parameters

### 3.8.2 Faraday cup

- **Repeller:** 15x15x3 mm metal plate, with 6 mm diameter hole in the centre
- **Collector:** Parallepipe of 15x15x10 mm with a conic hole of 6 mm in diameter in a centre of the front face. Cone inclination: 45°
- **Distance collector-repeller:** 2 mm
- **Repeller polarization**: up to -500 V

# 4 Prototype design and test in a dedicated helium ion source

The next step in the study of feasibility of the 4D emittance scanner is building a first prototype to verify is the design is correct and to check all the simulations and theoretical conclusions.

To achieve this, an ion source must be used. In particular, the CRISP ion source, previously used to test a 2D emittance scanner was selected. It is an ion source of positive helium ions, with a maximum energy of 2.5 keV, a total current under 1 mA, and a divergence of about 50 mrad for the acceleration voltage used [14].

The source is used to test a prototype of Faraday cup without the deflector, to check the design and investigate the effect of the voltage on the repeller and for test the performance of an amplifier circuit (variable gain low noise transimpedance current amplifier DLPCA-S3 of Femto) to check the signal noise in presence of RF source.

Then, a prototype of the entire scanner was built, to test all the functionalities of the object.

## 4.1 Experimental setup

The setup (**Figure 38**) consists of a vacuum chamber, where the prototypes are placed on a manipulator, that allows to move them in a region of the chamber were a beam of positive helium ions is generated by the source.

This source [14] (**Figure 39**) is composed by a glass tube were some helium at low pressure is injected. Around the tube, a winding of copper wire with several turns is present. A loop of thick wire is also around the tube, in which current at RF frequency (about 29 MHz) flows. This loop works like a primary winding of a transformer, inducing high voltage on the other winding, that form a capacitive coupling with the plasma inside glass container. At the end of the tube, there are three grids with seven holes in each one. The first grid is polarized to a negative voltage of about 1-2 kV, and the other two grid to ground potential. The third one may be polarized to focus the beam, but it was not used, and so it was connected to ground potential. So, ions are extracted from the plasma and accelerated towards the centre of the vacuum chamber.

For the experimental activity, the pressure in the chamber was brought to about $10^{-3}$ Pa. Then the helium was injected in the top part of the ion source, reaching a pressure of about 1 Pa to ignite the plasma. The pressure inside the central part of the vessel was of about 0.1 Pa.

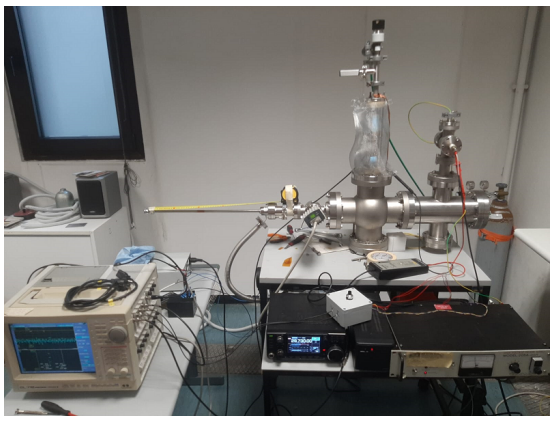

**Figure 38:** The entire laboratory setup for the measurement

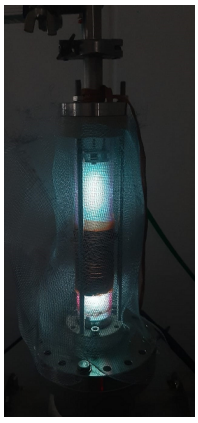

**Figure 39:** CRISP ion source

## 4.2 The Faraday cup prototype

The prototype of the Faraday cup (**Figure 40**) was built with two pieces of copper, that were held by a PLA plastic support that was made with 3D printing. Electrical connections were made with Kapton coated cables. The cup was secured to the manipulator with a metal bracket.

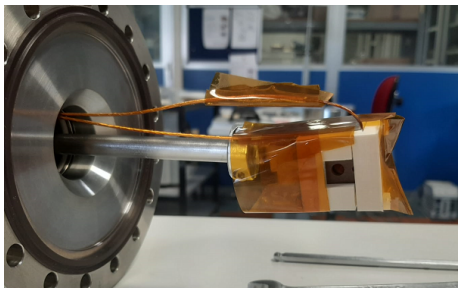

**Figure 40:** Prototype of the Faraday cup mounted on the manipulator

## 4.3 Repeller characterisation

The first measurement aims at investigating the effect of the repeller voltage on the current measure. The cup was located in front of the centre of the beam and stayed in this position during this part of the experiment. The voltage of the repeller was varied from 0 to -100 V and the corresponding current was acquired. Then, the voltage drop between the acceleration grids was varied, and the process was repeated for different beam proprieties. The acquired datasets are reported in **Table 1** with their conditions. Data are instead shown in **Figure 41**.

To provide an estimation of the error on current measure, a profile of the noise at fixed position of that cup was acquired (**Figure 42**). Half of the dispersion of the noise is the maximum error on current measures, that is about $\pm$ 7 nA, which is also a good estimation of the resolution of the current detector. It is far from initial goal of $\pm$ 1 nA, but it is a good start point for future development, also considering that the best resolution achieved from the Allison scanner during the SPIDER measurement campaign was $\pm$ 10 nA.

| dataset | $V_{acceler.}$ (V) | $I_{tot}$ (mA) | $p_{CRISP}$ (Pa) | $p_{vessel}$ (Pa) | $f_{RF}$ (MHz) |
|---|---|---|---|---|---|
| 1 | 777 | 0.50 | 2.03 | 0.0648 | 29.95 |
| 2 | 1445 | 0.69 | 2.03 | 0.0648 | 29.95 |
| 3 | 1924 | 0.75 | 2.03 | 0.0648 | 29.95 |

**Table 1:** Parameters for different datasets for repeller study

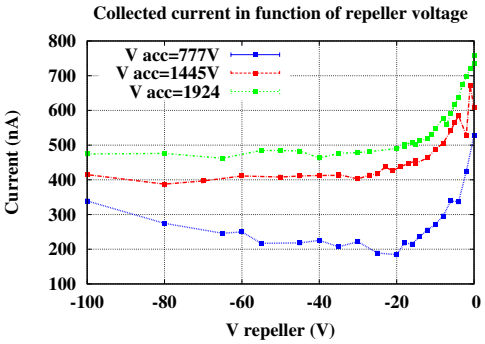


**Figure 41:** Repeller characterisation

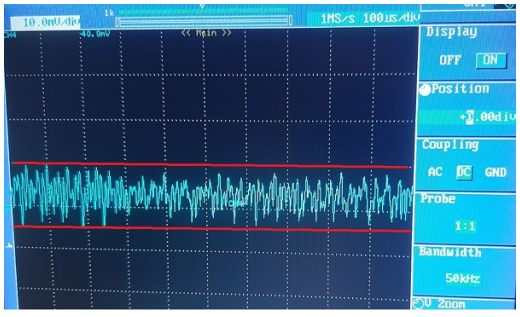


**Figure 42:** Signal noise at the output of the oscilloscope. One division is equal to 10 mV, which are 10 nA measured at the cup with a gain of $10^6$

The collected current is maximum when the repeller is turned off, due to the escaping of secondary electrons. Decreasing the voltage of the deflector reduces this phenomenon until the spurious current of electrons is totally repressed (about -40 V), and then the repeller voltage is little related to the current measured. This is well verified for the dataset at 1445 and 1924 V, and less for the one at 777 V.

A possible explanation of this is possibly due to the presence of an undesired small current between current and collector (only 100 nA) carried by some ionized particles of the helium gas in the vessel. This seems not to happen at higher energy of ions, maybe for the different ability

of ions to ionize the gas in the vessel. However, in view of SPIDER use, measurements at higher voltage are more significant, but the dataset at 777 V suggests that a better analysis of the distance between repeller and collector is needed.

## 4.4 Spatial profile measurement

The next measurement was done for checking the nature of the beam generated by the source. The Faraday cup was moved inside the vessel with the manipulator, and for each position the current was acquired. In this way, the spatial profile of the beam in one direction is acquired. The voltage on the repeller was set to -50 V. The experimental condition are written in **Table 2**.

| $V_{acceler.}$ (V) | $I_{tot}$ (mA) | $p_{CRISP}$ (Pa) | $p_{vessel}$ (Pa) | $f_{RF}$ (MHz) | $V_{rep}$ (V) |
|---|---|---|---|---|---|
| 2011 | 0.75 | 2.03 | 0.0642 | 28.92 | -50 |

**Table 2:** Experimental condition for the spatial characterisation of the beam

Three datasets were acquired (**Figure 43**) in different space region one at time. A Gaussian-like beam profile can be found as a function of distance. However, different datasets are not totally compatible with each other. This can have two explanations.

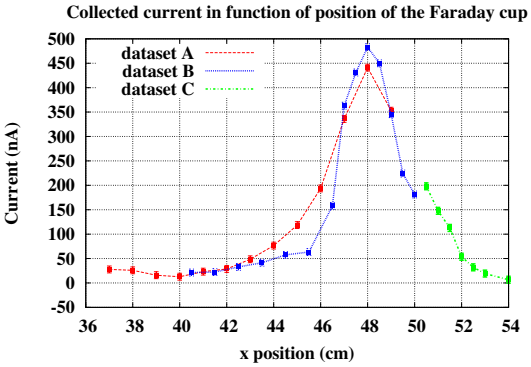


**Figure 43:** CRISP spatial profile distribution

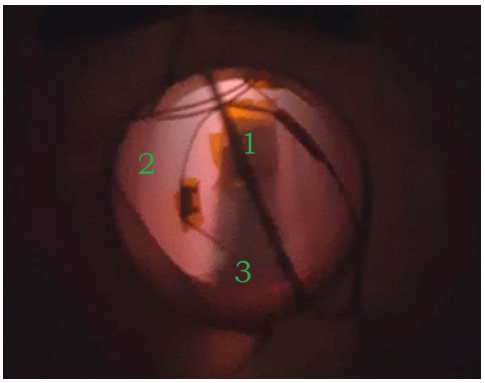


**Figure 44:** Photo of the inside of the vessel. 1 - Faraday cup 2 - ionized gas that reveals the beam 3 - the cup blocks a portion of the beam, casting a shadow

The first, is again the uncontrolled experimental condition, which can fluctuate when two datasets are acquired. For example, one issue can be the matching between the RF transmitter and the resonance frequency of the plasma, that changed a little in time and imposed to adjust the RF generator. Another possible explanation is given by thermal effects.

The second explanation, it that the measurement system is not stable, due to the presence of electric noise or potential induced on the electrode by the plasma. This is generated inside the vessel because the beam ionized the gas at low pressure.

## 4.5 Prototype of the entire scanner

The prototype of the Faraday cup was dismounted, and the one of the entire scanner was set in place (**Figure 45**). It was made by three pieces of PLA plastic that were made with 3D printing, that form a deflector box and a housing for the Faraday cup (**Figure 46**).

The cup was equal to the previous prototype, with the same pieces of metal put in the new piece of plastic. The plates were made by pasting some copper tape inside the deflector box. The electric contact was granted by some through screws, and the four plates were collected to four separate voltage generators.

A metal plate with a hole was placed before the Faraday cup to select particles. Another plate with a hole was attached at the front side of the deflector box. These two last plates were connected

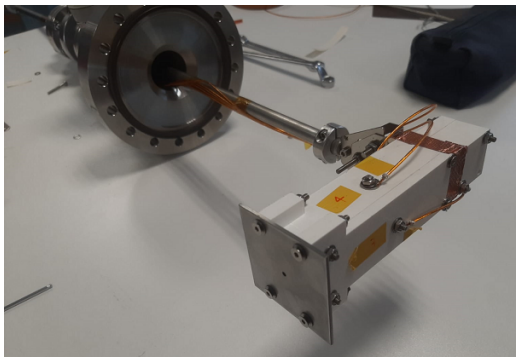

**Figure 45:** Prototype of the 4D emittance scanner on a manipulator. The handling system can move it only in one spatial direction

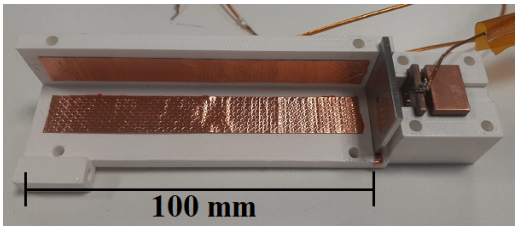


**Figure 46:** Inside of the prototype of the scanner. From the left, the plates, the rear wall of the deflector, the repeller and the collector can be seen. The front wall was taken apart to open the plastic support

to ground. After connecting the repeller and collector, everything was secured to the manipulator with a metal bracket and screws.

The dimensions of the scanner were not the same for SPIDER, but the parameters were adjusted to the CRISP source and to the available space in the vessel. A length $L$ of 100 mm and a radius of hole $R$ of 1.2 mm were chosen. These parameters are suitable for a check of the main theoretical concepts of the diagnostic, and it is not intended to measure precisely the beam proprieties.

## 4.6 Measurement problems with the entire scanner prototype

This prototype was expected to measure a current distribution as a function of the voltages applied at the plates, and this expected to change for different space position. However, the current measurements were not possible because they were too unstable. This was caused by two reasons.

In first place, the plate drivers were made by several devices (generators, control board, Raspberry boards for remote control of the signal in time). These components introduced a bigger electric noise on the electrical line, that was not present in the previous measurement.

The second problem is the Faraday screening: the plates worked as a channel for electric noise to affect the collector measurement, due to the short distance between the cup and the plates.

So, it is necessary to improve the screening of the prototype with a metal cover connected to ground. Another possible improvement is to upgrade the ground connection of the experiment: the instabilities were reduced (but not removed) be reorganized the electrical connections of the experiment bringing the ground connection directly on the vessel.

These instabilities do not compromise the feasibility of the 4D scanner, but for obtaining results from this prototype a new design of the experimental setup is necessary, considering the previous issues.

# 5 Conclusions and future work

The feasibility study of the 4D emittance scanner provided promising results. A theoretical model suggests some optimal parameters for the scanner, in order to achieve angular and spatial resolution suitable for measuring in SPIDER and detectable currents, with a length of 200 mm and hole size of 0.5 mm. However, to include the effect of a real electric field, of the Gaussian distribution of the beam and of the deflector with round holes (R = 0.25 mm), a numerical simulation in MATLAB was performed.

The simulation confirms that the currents, although low, should be measurable and that a voltage-angle relation holds. But the simulation did not take into account the fringe field effect in the end regions of the deflector, and so another simulation in COMSOL was performed, showing that this effect has a small influence.

The same simulation also showed how a distance of 3 mm of plates from the front and rear walls of the deflector did not affect meaningfully the deflection ability of the scanner. Distance between opposite plates was chosen to analyze large angles (until 100 mrad). The distance between plates and case was set to 3 mm to avoid discharge in vacuum.

A first design of the Faraday cup was proposed, and it was tested with the CRISP ion source also to verify the maximum error obtained on current measures, that is equal to ± 7 nA.

The Faraday cup resolution must be improved by less than an order of magnitude. This can be done by adding a screen against the electric noise, but also with a different amplifier design. For example, an internal preamplifier can process the signal, that at the output is higher and less sensitive to the electric noise in the cable toward the principal amplifier. Alternatively a channeltron to multiply the collected current can be considered.

The experimental setup has to be improved to test the scanner prototype; it can allow to check all the information provided by theory and simulations, and can also point out new effects that were not taken in account.

To verify the feasibility, it is also important to consider the design of the handling system and the resistance to heat loads of the detector, which will be investigated in the future.

# References


[1] https://www.iter.org/

[2] V. Toigo et al. , *"The PRIMA test facility: SPIDER and MITICA test-beds for ITER neutral beam injectors"*, New Journal of Physics, vol. 19, no. 8, 2017. [Online] available: https://doi.org/10.1088

[3] D. Marcuzzi, P. Agostinetti, M. Dalla Palma, F. Degli Agostini, M. Pavei, A. Rizzolo, M. Tollin, and L. Trevisan, *"Detail design of the beam source for the spider experiment"*, Fusion Engineering and Design, vol. 85, no. 10-12, pp. 1792–1797, 2010. [Online] available: https://doi.org/10.1016/j.fusengdes.2010.05.039

[4] Paul W. Allison, Joseph D. Sherman, and David B. Holtkamp, *An emittance scanner for intense low-energy ion beams*, IEEE Transactions on Nuclear Science, Vol. NS-30, No. 4, 1983

[5] Kalvas *"Beam Extraction and Transport"*, Department of Physics, University of Jyväskylä, 2013

[6] M. Reiser, *Theory and Design of Charged Particle Beams*, Wiley-VCH Verlag GmbH & Co KGaA, 2nd Edition (2008), ISBN 978-3-527-40741-5

[7] V. Toigo et al. *Lessons learned after three years of SPIDER operation and the first MITICA integrated tests* Fusion Engineering and Design 191 113590, 2023

[8] G Serianni et al *Neutralisation and transport of negative ion beams: physics and diagnostics* New J. Phys. 19 045003, 2017 [Online] available: https://iopscience.iop.org/article/10.1088/1367-2630/aa64bd/meta

[9] Michael A. Lieberman, Alan J. Lichtenberg, *"Principles of Plasma Discharges and Materials Processing"*, WileyBlackwell; 2nd Edition (13 May 2005), ISBN 0-471-72001-1, Table 14.1, pag.545

[10] Eifionydd Jones and F Llewellyn Jones, *"Theory of Secondary Emission of Electrons in Hydrogen"*, Proceedings of the Physical Society, Volume 80, Number 2, 1962 [Online] available: https://iopscience.iop.org/article/10.1088/0370-1328/80/2/312

[11] https://it.mathworks.com/products/matlab.html?s_tid=hp_products_matlab

[12] https://www.comsol.it/

[13] C. Poggi, E. Sartori, M. Tollin, M. Brombin,1 M. Zaupa, E. Fagotti and G. Serianni *Design and development of an Allison type emittance scanner for the SPIDER ion source* Rev. Sci. Instrum. 91, 013328, 2020

[14] C. Poggi, E. Sartori, M. Zuin, M. Brombin,V. Cervaro, M. Fadone, A. Fassina, M. Fincato, B. Segalini and G. Serianni, *"CRISP: a Compact RF Ion Source Prototype for emittance scanner testing"*, Rev. Sci. Instrum. 91, 033314, 2020

# 6 Appendix

## 6.1 Analytic calculation of acceptance and resolutions

**Acceptance**

$$A = \int_{d\Omega} dx_0 dx_0' dy_0 dy_0' = \int_{-\frac{s}{2}}^{\frac{s}{2}} dx_0 \int_{\frac{1}{L}(-\frac{h}{2}-x_0)}^{\frac{1}{L}(\frac{h}{2}-x_0)} dx_0' \int_{-\frac{s}{2}}^{\frac{s}{2}} dy_0 \int_{\frac{1}{L}(-\frac{h}{2}-y_0)}^{\frac{1}{L}(\frac{h}{2}-y_0)} dy_0' = \left( \int_{-\frac{s}{2}}^{\frac{s}{2}} dx_0 \int_{\frac{1}{L}(-\frac{h}{2}-x_0)}^{\frac{1}{L}(\frac{h}{2}-x_0)} dx_0' \right)^2 =$$

$$= \left( \frac{1}{L} \int_{-\frac{s}{2}}^{\frac{s}{2}} dx_0 \, \frac{h}{2} - x_0 + \frac{h}{2} + x_0 \right)^2 = \left[ \frac{h}{L} (\frac{s}{2} + \frac{s}{2}) \right]^2 = \frac{s^2 h^2}{L^2}$$

**Spatial resolution**

$$var(x_0) = \frac{\int_{d\Omega} {x_0}^2 \, dx_0 dx_0' dy_0 dy_0'}{\int_{d\Omega} dx_0 dx_0' dy_0 dy_0'} = \frac{\int_{-\frac{s}{2}}^{\frac{s}{2}} {x_0}^2 \, dx_0 \int_{\frac{1}{L}(-\frac{h}{2}-x_0)}^{\frac{1}{L}(\frac{h}{2}-x_0)} dx_0' \int_{-\frac{s}{2}}^{\frac{s}{2}} dy_0 \int_{\frac{1}{L}(-\frac{h}{2}-y_0)}^{\frac{1}{L}(\frac{h}{2}-y_0)} dy_0'}{\int_{-\frac{s}{2}}^{\frac{s}{2}} dx_0 \int_{\frac{1}{L}(-\frac{h}{2}-x_0)}^{\frac{1}{L}(\frac{h}{2}-x_0)} dx_0' \int_{-\frac{s}{2}}^{\frac{s}{2}} dy_0 \int_{\frac{1}{L}(-\frac{h}{2}-y_0)}^{\frac{1}{L}(\frac{h}{2}-y_0)} dy_0'} =$$

$$= \frac{\int_{-\frac{s}{2}}^{\frac{s}{2}} {x_0}^2 \, dx_0 \int_{\frac{1}{L}(-\frac{h}{2}-x_0)}^{\frac{1}{L}(\frac{h}{2}-x_0)} dx_0'}{\int_{-\frac{s}{2}}^{\frac{s}{2}} dx_0 \int_{\frac{1}{L}(-\frac{h}{2}-x_0)}^{\frac{1}{L}(\frac{h}{2}-x_0)} dx_0'} = \frac{L}{sh} \int_{-\frac{s}{2}}^{\frac{s}{2}} {x_0}^2 \frac{h}{L} \, dx_0 = \frac{1}{s} \int_{-\frac{s}{2}}^{\frac{s}{2}} {x_0}^2 \, dx_0 = \frac{1}{3s} (\frac{s^3}{8} + \frac{s^3}{8}) = \frac{s}{12}$$

$$\implies \sigma_{x_0} = \sqrt{var(x_0)} = \frac{s}{\sqrt{12}}$$

**Angular resolution**

$$var(x_0') = \frac{\int_{d\Omega} {x_0'}^2 \, dx_0 dx_0' dy_0 dy_0'}{\int_{d\Omega} dx_0 dx_0' dy_0 dy_0'} = \frac{\int_{-\frac{s}{2}}^{\frac{s}{2}} dx_0 \int_{\frac{1}{L}(-\frac{h}{2}-x_0)}^{\frac{1}{L}(\frac{h}{2}-x_0)} {x_0'}^2 dx_0' \int_{-\frac{s}{2}}^{\frac{s}{2}} dy_0 \int_{\frac{1}{L}(-\frac{h}{2}-y_0)}^{\frac{1}{L}(\frac{h}{2}-y_0)} dy_0'}{\int_{-\frac{s}{2}}^{\frac{s}{2}} dx_0 \int_{\frac{1}{L}(-\frac{h}{2}-x_0)}^{\frac{1}{L}(\frac{h}{2}-x_0)} dx_0' \int_{-\frac{s}{2}}^{\frac{s}{2}} dy_0 \int_{\frac{1}{L}(-\frac{h}{2}-y_0)}^{\frac{1}{L}(\frac{h}{2}-y_0)} dy_0'} =$$

$$\frac{\int_{-\frac{s}{2}}^{\frac{s}{2}} dx_0 \int_{\frac{1}{L}(-\frac{h}{2}-x_0)}^{\frac{1}{L}(\frac{h}{2}-x_0)} {x_0'}^2 dx_0'}{\int_{-\frac{s}{2}}^{\frac{s}{2}} dx_0 \int_{\frac{1}{L}(-\frac{h}{2}-x_0)}^{\frac{1}{L}(\frac{h}{2}-x_0)} dx_0'} = \frac{L}{3sh} \int_{-\frac{s}{2}}^{\frac{s}{2}} \frac{1}{L^3} [(\frac{h}{2} - x_0)^3 - (-\frac{h}{2} + x_0)^3] \, dx_0 = \frac{1}{3sL^2} \int_{-\frac{s}{2}}^{\frac{s}{2}} \frac{h^2}{4} + 3{x_0}^2 \, dx_0 =$$

$$= \frac{1}{3sL^2} \left( \frac{h^2 s}{4} + \frac{s^3}{4} \right) = \frac{h^2 + s^2}{12L^2} \implies \sigma_{x_0'} = \sqrt{var(x_0')} = \frac{\sqrt{h^2 + s^2}}{\sqrt{12} L}$$

## 6.2 Taylor expansion of the solution of the differential equation to solve self divergence of the beam

$$r^I = \frac{dr(z)}{dz}, r^{II} = \frac{d^2 r(z)}{dz^2}, ...$$

$$r^{II} = \frac{k}{r} \xrightarrow{\frac{d}{dt}} r^{III} = -\frac{k}{r^2} r I \xrightarrow{\frac{d}{dt}} r^{IV} = K \left( \frac{2}{r^3} r^I r^I - \frac{1}{r^2} r^{II} \right)$$

$$r|_{z=0} = 0 \quad r^I|_{z=0} \quad r^{II}|_{z=0} = \frac{k}{r_0} \quad r^{III}|_{z=0} = 0 \quad r^{IV}|_{z=0} = -\frac{k^2}{{r_0}^3}$$

$$r(z) = r|_{z=0} = 0 + r^I|_{z=0} \, z + \frac{1}{2} r^{II}|_{z=0} \, z^2 + \frac{1}{6} r^{III}|_{z=0} \, z^3 + \frac{1}{24} r^{IV}|_{z=0} \, z^4 + ...$$

$$r(z) = r_0 + \frac{1}{2} \frac{k}{r_0} z^2 - \frac{1}{24} \frac{K^2}{{r_0}^3} z^4 + o(z^6)$$

The precision of the expansion is $o(z^6)$ because the fifth term is equal to zero, like the other odd terms of the expansion. In fact, the solution bust be an even function, because the problem must be symmetrical for negative value of $z$.